Side-by-side ZnSe/ZnCdSe Bicrystalline Nanoribbons Prepared by a Two-Step Process

ARTICLE *in* THE JOURNAL OF PHYSICAL CHEMISTRY C · OCTOBER 2007

Impact Factor: 4.77 · DOI: 10.1021/jp074789c

3 AUTHORS, INCLUDING:

Chong-Xin Shan
Chinese Academy of Sciences
168 PUBLICATIONS **2,557** CITATIONS

Side-by-side ZnSe/ZnCdSe Bicrystalline Nanoribbons Prepared by a Two-Step Process

Z. Liu, C. X. Shan, and S. K. Hark*

Department of Physics, The Chinese University of Hong Kong, Shatin, Hong Kong

L. P. You and J. Chen

Electron Microscopy Laboratory, School of Physics, Peking University, Beijing, China

Received: June 20, 2007; In Final Form: August 8, 2007

By a two-step method, side-by-side bicrystalline ZnSe/ZnCdSe nanoribbons were fabricated via metalorganic chemical vapor deposition. The nanoribbons were characterized by secondary and transmission electron microscopy, and energy dispersed X-ray spectroscopy. A good epitaxial relationship and a sharp interface exist between the two crystals, despite their different crystalline orientation and composition. The lattice mismatch induced strain is fully accommodated by bending. Two mechanisms, the vapor−liquid−solid mechanism and a subsequent asymmetric epitaxy, are involved in the growth of the bicrystals. Our results show that the two-step methods, which were commonly used to fabricate core−shell and axial heterostructures, can also yield bicrystals.

Introduction

Recently, there has been considerable interest in fabricating one-dimensional (1D) nanoheterostructures, such as axially heterostructured nanowires,[1,2] core−shell nanocables,[3] nanobranches,[4] and bicrystalline nanostructures.[5−7] Successful fabrications have been demonstrated in metal oxides and various semiconductors of groups IV, II−VI, and III−V, using laser assisted catalytic growth,[1] molecular beam epitaxy,[2] chemical vapor deposition,[3] metalorganic chemical vapor deposition (MOCVD),[4] and thermal evaporation.[5,6] Novel properties, such as quantum confinement,[8] Coulomb blockade,[9] and long carrier mean free path, have also been observed in the 1D nanoheterostructures.[10] Although one-step syntheses can sometimes yield heterostructures,[11] two-step fabrications offer more flexibility in combining different materials and allow separate controls over each material. For example, in the two-step growth of nanocables, the diameter of the core and the thickness of the sheath are completely independent to each other. Similarly, the widths of the barrier and the well in a superlattice nanowire are also independent. Despite these innate advantages, few two-step syntheses of 1D bicrystals have been reported.[7,12,13] This may be related to the difficulty in achieving asymmetric, side-by-side growth at the second step.

ZnSe, CdSe, and their alloys are direct, wide-band gap semiconductors commonly used in optoelectronics, and as biochemical detectors. Many ZnSe−CdSe heterostructures including quantum wells,[14] quantum dots,[15] and superlattices[16] have been formed and studied. Although ZnSe, CdSe, and even ZnCdSe alloy nanowires and nanoribbons have also been fabricated recently,[17−20] 1D heterostructures of this system have rarely been.[21] In this paper, we report a form of ZnSe/ZnCdSe bicrystalline nanoribbons prepared in two steps by MOCVD and discuss the mechanism of the asymmetric epitaxial growth observed in the second step that results in the side-by-side heterostructure.

* Author to whom correspondence should be addressed. E-mail: skhark@phy.cuhk.edu.hk.

In the first step we fabricated the wurtzite-structured ZnCdSe alloy nanowires. The experimental conditions for this are similar to those in our earlier reports.[19,22] Briefly, the nanowires were grown on GaAs (100) substrates, sputter-coated with a thin layer (∼20 nm thick) of Au to serve as catalysts, using diethylzinc, dimethylcadmium, and diisopropylselenide as precursors and 7N hydrogen as a carrier gas. The growth temperature and duration of this step were 480 °C and 2400 s. There was a period of 300 s of interruption during which the flows of precursors were switched off and the temperature lowered to 400 °C. In the second step, using only diethylzinc and diisopropylselenide, we grew wurtzite-structured ZnSe[23] on one side of the ZnCdSe nanowires epitaxially for 600 s. The growth pressure was kept at 500 Torr for both steps. A control sample of alloy nanowires grown without the second step was also fabricated for comparison. The as-synthesized nanostructures were studied by scanning and transmission electron microscopy (SEM, using Leo 1450VP, TEM, using Philips CM120 and Tecnai 20). Their chemical compositions were profiled in a scanning transmission electron microscope (STEM, Tecnai F30).

The morphology of the bicrystalline nanoribbons and the ZnCdSe nanowires from which they evolve are shown in Figure 1. A large number of curved nanoribbons are seen covering the GaAs substrate in the SEM image (Figure 1a). Their side-by-side bicrystalline nature is revealed by the low-magnification TEM image in (Figure 1b). The darker contrast arises from the stronger scattering of electrons by Cd atoms in comparison with Zn atoms. As evidenced by the straight ZnCdSe nanowire in the control sample (Figure 1c), the bending of the nanoribbons only occurs after the second-step growth. From the electron microscopy, we found that about 80% of the products of the two-step growth are these bicrystalline nanoribbons, whose typical dimensions are 3−5 μm in length and 60−100 nm in width. A lattice resolved HRTEM image zooming in on the interfacial region of a single nanoribbon is shown in Figure 2a. It reveals the abrupt interface of two phases, which are different not only in their crystalline orientation but also in their composition. After examining the interfacial regions of many

10.1021/jp074789c CCC: $37.00
Published on Web 10/11/2007

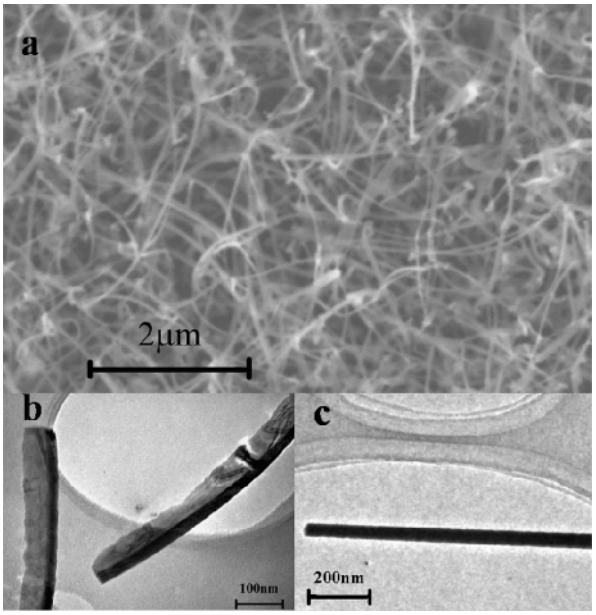

Figure 1. (a) SEM plan view of the bicrystalline nanoribbons. (b) TEM image of two bicrystalline nanoribbons. (c) A TEM image of a ZnCdSe nanowire formed after the first step of growth.

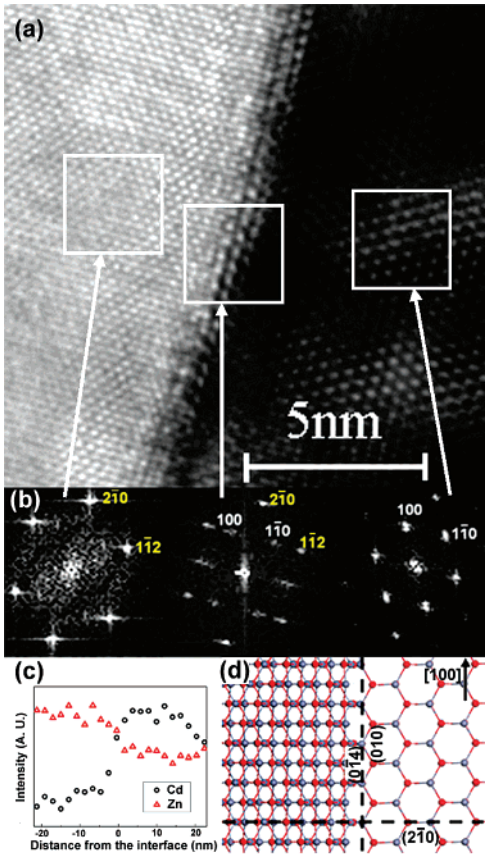

Figure 2. (a) HRTEM image of the interfacial region of a single bicrystalline nanoribbon. (b) FFT patterns of different regions indicated by the arrows near the interface. The leftmost belongs to the [241] zone of a wurtzite lattice, the rightmost to [001], and the center is a combination of the two. (c) Elemental profiles of cations across the interface. (The intensity is normalized.) (d) Lattice model showing the epitaxial relationship. The dashed lines indicate the relationship $(2\bar{1}0)_{ZnSe}//(2\bar{1}0)_{ZnCdSe}$ and $(0\bar{1}4)_{ZnSe}//(010)_{ZnCdSe}$ and the arrow shows the [100] direction.

nanoribbons, we concluded that they contain a very low density of misfit dislocations. The profiles of cations across the interface

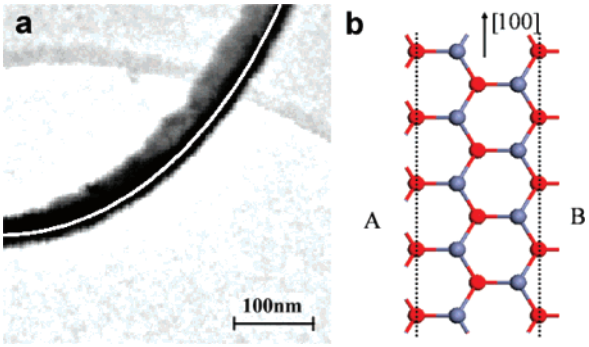

Figure 3. (a) TEM image of a bicrystalline nanoribbon. The white line superimposed on the nanoribbon is the projection of the fitted circular arc. (b) The atomic configuration of the wurtzite (001) layers showing the two different (010) planes labeled as A and B.

are shown in Figure 2c, which reveals that the lighter and darker region in Figure 2a corresponds to the ZnSe and ZnCdSe phase, respectively. Quantitative analyses of the EDX spectra (not shown) determine that the latter phase has a composition in which the Zn fraction ranges from 0.43 to 0.66, depending on the nanoribbons. The heteroepitaxial relationship of the two phases is demonstrated by the fast Fourier transform (FFT) patterns shown in Figure 2b. The left and right patterns belong to different zones of the wurtzite structure. The two patterns share the common $(2\bar{1}0)$ and $(\bar{2}10)$ spots. The pattern in the middle, which is a superposition of the ones on the left and right, shows that the common spots completely overlap, indicating the unusual, but excellent, epitaxial relationship between the two phases. It is obtained through a slight dilation and a concomitant contraction of the interplanar distance $d_{2\bar{1}0}$ (2.05 Å) in the ZnSe and ZnCdSe phase, respectively, in comparison with the corresponding bulk material. The epitaxial relationship is more clearly illustrated by the lattice model shown in Figure 2d. The atomic planes normal to the [100] direction are $(2\bar{1}0)$ in both phases. The interface is the $(0\bar{1}4)/(010)$ plane when referred to the ZnSe/ZnCdSe phase. The calculated lattice mismatch is between 2.5% and 4.3%, depending on the Zn content in ZnCdSe.

The mismatch induces elastic strain in the bicrystalline nanoribbons, which is evidenced by their bent shape. The radius of curvature of the nanoribbon is related to the strain, as in the bending of a beam. Assuming the nanoribbon is bent into a circular arc, we may find their radius of curvature by fitting the curved shape. Figure 3a shows an example of the curve fittings to the nanoribbons. In the TEM observations, the image obtained is a projection of the nanoribbon onto the image plane. The angle between the image plane and the plane that actually contains the circular arc varies for each nanoribbon and is therefore considered as an adjustable parameter, in addition to the radius of curvature R, in the fitting. The white line superimposed on the nanoribbon is the fitted projection of a circular arc having a radius R of (600 ± 30) nm. Since the width w of the nanoribbon is about 60 nm, its bending strain, as estimated from $w/2R$, is $(5 \pm 1)\%$. The facts that the bending strain agrees with the lattice mismatch and that a low density of dislocations is found at the interface indicate that the lattice mismatch induced strain is fully accommodated by the bending. Additional experimental evidence is supplied from the observations that nanoribbons can be straightened by electron beam induced radiation damage, which relaxes their strain through the creation of grain boundaries and other defects.

The growth of the bicrystalline nanoribbons involves two different mechanisms. In the first step, straight wurtzite-

structured ZnCdSe nanowires grow up on the gold-coated GaAs substrate via the VLS (vapor−liquid−solid) mechanism. The VLS mechanism ceases to be operative below the solidification temperature of the alloy droplets. Apparently, 400 °C is too low for the Au−Zn−Cd alloy droplets to exist as a liquid, even when their nanosized dimension is taken into consideration. The subsequent epitaxial growth of ZnSe on one of the bounding surfaces of the ZnCdSe nanowires results in the formation of the ZnSe/ZnCdSe bicrystalline nanoribbons. It is interesting that ZnSe should appear on only one side of the nanowires in the second step. Had it grown around the nanowire, ZnSe/ZnCdSe core−shell nanocables would have resulted. In the one-step method of growth, formation of bicrystals is usually induced by catalysts found at the interface between the two constituent crystals.[5,6] Since we did not find any evidence of impurity particles or phases at the interface of our bicrystalline nanoribbons, their formation is probably not induced by catalysts. A shadowing effect has been used to explain the one-sided deposition that results in bicrystalline TiO_2/SnO_2 nanoribbons.[13] We note that the lattice mismatch induced strain always leads to bent bicrystalline nanoribbons in which the ZnSe phase forms the inner circular arc, as observed in their TEM images. If the one-sided growth were caused by shadowing, the nanoribbons would have bent toward a single direction—the flow direction of the precursors. In the SEM image of Figure 1a, it is quite apparent that the bending direction is random, indicating the insignificance of the shadowing effect under our MOCVD conditions. In ZnO nanostructures, a self-catalytic effect has been invoked to explain the preferential one-sided growth on Zn-terminated polar surfaces.[24] The common polar surfaces are {001} and {011} in the wurtzite structure. The interface of our ribbons, when referred to the ZnCdSe phase, is the (010) plane, which contains an equal density of cations and anions, and is therefore not a polar surface. Thus, the polar explanation is also not suitable for the one-sided growth in our bicrystalline nanoribbons. We suggest that the difference in the densities of dangling bonds of the {010} planes is responsible for the one-sided growth in our case. A similar discussion has been used to explain the island growth of GaN.[25] Figure 3b shows the atomic configuration of wurtzite (001) layers. As the direction of growth of ZnCdSe in the first step (VLS mode) is along [100], two of the {010} planes, labeled as A and B, become the bounding side surfaces. On the A planes, there are two dangling bonds per atom; and on the B planes there is only one. So the A planes are more reactive than the B planes. In the second step, growth along [100] is stunted by the solidification of the catalytic droplets, leaving the A plane as the preferred site for ZnSe epitaxy. This one-sided epitaxy thus leads to the formation of the bent bicrystalline nanoribbons. Moreover, we found a growth interruption is needed for fabricating these bicrystalline nanoribbons. Hydrogen that is prevalent in the MOCVD process is perhaps playing a role in helping the ZnSe epitaxy on the ZnCdSe (010) surface.

In summary, side-by-side ZnSe/ZnCdSe bicrystalline nanoribbons have been fabricated by a two-step process by using MOCVD. The two crystalline phases share an abrupt interface and are different not only in their crystal orientations but also in their compositions. The lattice mismatch between them is accommodated by bending. A uncommon, nearly dislocation free, epitaxial relationship, $(2\bar{1}0)_{ZnSe}//(2\bar{1}0)_{ZnCdSe}$ and $(0\bar{1}4)_{ZnSe}//(010)_{ZnCdSe}$, is observed between the two phases. Two growth mechanisms are involved in the growth of the nanoribbons. The VLS mechanism in the first step yields ZnCdSe nanowires that serve as the substrates for ZnSe epitaxy in the second step. The asymmetry in the density of dangling bonds on the bounding {100} planes explains the one-sided epitaxy that leads to bicrystals instead of nanocables.

Acknowledgment. We thank Prof. Quan Li for helpful discussions. The work in this paper was partially supported by grants from the Research Grants Council of the Hong Kong Special Administrative Region, China (Project No. CUHK 401003), and a CUHK Direct Grant (Project No.2060305).

References and Notes

(1) Gudiksen, M. S.; Lauhon, L. J.; Wang, J. F.; Smith, D. C.; Lieber, C. M. *Nature* (*London*) **2002**, *415*, 617.
(2) Bjork, M. T.; Ohlsson, B. J.; Sass, T.; Persson, A. I.; Thelander, C.; Magnusson, M. H.; Deppert, K.; Samuelson, L. *Appl. Phys. Lett.* **2002**, *80*, 1058.
(3) Lauhon, L. J.; Gudiksen, M. S.; Wang, D. L.; Lieber, C. M. *Nature* (*London*) **2002**, *420*, 57.
(4) Tak, Y. J.; Ryu, Y. H.; Yong, K. *Nanotechnology* **2005**, *16*, 1712.
(5) Zou, K.; Qi, X. Y.; Duan, X. F.; Zhou, S. M.; Zhang, X. H. *Appl. Phys. Lett.* **2005**, *86*, 013103.
(6) Meng, X. M.; Jiang, Y.; Liu, J.; Lee, C. S.; Bello, I.; Lee, S. T. *Appl. Phys. Lett.* **2003**, *83*, 2244.
(7) Yin, L. W.; Li, M. S.; Bando, Y.; Golberg, D.; Yuan, X.; Sekiguchi, T. *Adv. Funct. Mater.* **2007**, *17*, 270.
(8) Park, W. I.; Yi, G. C.; Kim, M.; Pennycook, S. J. *Adv. Mater.* **2003**, *15*, 526.
(9) Thelander, C.; Martensson, T.; Bjork, M. T.; Ohlsson, B. J.; Larsson, M. W.; Wallenberg, L. R.; Samuelson, L. *Appl. Phys. Lett.* **2003**, *83*, 2052.
(10) Lu, W.; Xiang, J.; Timko, B. P.; Wu, Y.; Lieber, C. M. *Proc. Natl. Acad. Sci. U.S.A.* **2005**, *102*, 10046.
(11) Wang, C.; Wang, J.; Li, Q.; Yi, G. C. *Adv. Funct. Mater.* **2005**, *15*, 1471.
(12) Hu, J.; Bando, Y.; Liu, Z.; Sekiguchi, T.; Golberg, D.; Zhan, J. *J. Am. Chem. Soc.* **2003**, *125*, 11306.
(13) He, R.; Law, M.; Fan, R.; Kim, F.; Yang, P. *Nano lett.* **2002**, *2*, 1109.
(14) Ku, J. T.; Kuo, M. C.; Shen, J. L.; Chiu, K. C.; Yang, T. H.; Luo, G. L.; Chang, C. Y.; Lin, Y. C.; Fu, C. P.; Chuu, D. S.; Chia, C. H.; Chou, W. C. *J. Appl. Phys.* **2006**, *99*, 063506.
(15) Zhang, B. P.; Li, Y. Q.; Yasuda, T.; Wang, W. X.; Segawa, Y.; Edamatsu, K.; Itoh, T. *Appl. Phys. Lett.* **1998**, *73*, 1266.
(16) Vodopyanov, L. K.; Kozyrev, S. P.; Sadofyev, Y. G.; Tarasov, G. G.; Litvinchuk, A. P. *Solid State Commun.* **2002**, *122*, 21.
(17) Zhang, X. T.; Liu, Z.; Leung, Y. P.; Li, Q.; Hark, S. K. *Appl. Phys. Lett.* **2003**, *83*, 5533.
(18) Shan, C. X.; Liu, Z.; Hark, S. K. *Nanotechnology* **2005**, *16*, 3133.
(19) Shan, C. X.; Liu, Z.; Hark, S. K. *Appl. Phys. Lett.* **2007**, *90*, 193123.
(20) Shan, C. X.; Liu, Z.; Ng, C. M.; Hark, S. M. *Appl. Phys. Lett.* **2005**, *87*, 033108.
(21) Solanki, R.; Huo, J.; Freeouf, J. L.; Miner, B. *Appl. Phys. Lett.* **2002**, *81*, 3864.
(22) Zhang, X. T.; Liu, Z.; Li, Quan; Hark, S. K. *J. Phys. Chem. B* **2005**, *109*, 17913.
(23) Shan, C. X.; Liu, Z.; Zhang, X. T.; Wong, C. C.; Hark, S. *Nanotechnology* **2006**, *17*, 5561.
(24) Wang. Z. L.; Kong, X. Y.; Ding, Y.; Gao, P.; Hughes, W. L.; Yang, R.; Zhang, Y. *Adv. Funct. Mater.* **2004**, *14*, 943.
(25) Xie, M. H.; Seutter, S. M.; Zhu, W. K.; Zheng, L. X.; Wu, H.; Tong, S. Y. *Phys. Rev. Lett.* **1999**, *82*, 2749.